



Farnsworth, A., Lunt, D., O'Brien, C., Foster, G., Inglis, G., Markwick, P., Pancost, R., & Robinson, S. A. (2019). Climate sensitivity on geological timescales controlled by nonlinear feedbacks and ocean circulation. *Geophysical Research Letters*.
<https://doi.org/10.1029/2019GL083574>

Peer reviewed version

Link to published version (if available):
[10.1029/2019GL083574](https://doi.org/10.1029/2019GL083574)

[Link to publication record in Explore Bristol Research](#)
PDF-document

This is the author accepted manuscript (AAM). The final published version (version of record) is available online via American Geophysical Union at <https://agupubs.onlinelibrary.wiley.com/doi/full/10.1029/2019GL083574> . Please refer to any applicable terms of use of the publisher.

University of Bristol - Explore Bristol Research

General rights

This document is made available in accordance with publisher policies. Please cite only the published version using the reference above. Full terms of use are available:
<http://www.bristol.ac.uk/red/research-policy/pure/user-guides/ebr-terms/>

1 **Climate sensitivity on geological timescales controlled**
2 **by non-linear feedbacks and ocean circulation**

3 **A. Farnsworth¹, D. J. Lunt¹, C. O'Brien², G. L. Foster³, G. N. Inglis⁴, P.**
4 **Markwick⁵, R. D. Pancost⁴, S. A. Robinson⁶**

5 ¹School of Geographical Sciences and Cabot Institute, University of Bristol, UK

6 ²Department of Geology and Geophysics, Yale University, USA

7 ³Ocean and Earth Science, University of Southampton, UK

8 ⁴School of Earth Sciences, School of Chemistry, and Cabot Institute, University of Bristol, UK

9 ⁵Knowing Earth Ltd, UK

10 ⁶Department of Earth Sciences, University of Oxford, UK

11 **Key Points:**

- 12 • Climate sensitivity on geological timescales depends on continental configuration
- 13 • Ocean area and ocean circulation non-linearly determine climate and climate sen-
- 14 sitivity
- 15 • Past climate sensitivity is not necessarily a good analogue for future climate sen-
- 16 sitivity

Corresponding author: Daniel J. Lunt, d.j.lunt@bristol.ac.uk

Abstract

Climate sensitivity is a key metric used to assess the magnitude of global warming given increased CO₂ concentrations. The geological past can provide insights into climate sensitivity; however, on timescales of millions of years, factors other than CO₂ can drive climate, including paleogeographic forcing and solar luminosity. Here, through an ensemble of climate model simulations covering the period 150-35 million years ago, we show that climate sensitivity to CO₂ doubling varies between ~3.5-5.5°C through this time. These variations can be explained as a non-linear response to solar luminosity, evolving surface albedo due to changes in ocean area, and changes in ocean circulation. The work shows that the modern climate sensitivity is relatively low in the context of the geological record, as a result of relatively weak feedbacks due to a relatively low CO₂ baseline, and the presence of ice and relatively small ocean area in the modern continental configuration.

1 Introduction

Climate sensitivity, in its very broadest terms, is a measure of the response of the climate system to an external forcing. More specifically, it is defined as the global annual mean near-surface air temperature equilibrium response to a defined forcing, usually either 1 Wm⁻² (e.g. PALAEOSENS Project Members, 2012) or a doubling of CO₂ (~3.7 Wm⁻², e.g. Charney et al., 1979). Despite (or perhaps due to) its simplicity, it is a widely used metric, and is a key variable in many impact (e.g. Donner, Skirving, Little, Oppenheimer, & Hoegh-Guldberg, 2005), policy (e.g. Rogelj, Meinshausen, Sedlacek, & Knutti, 2014), and economic (e.g. Hope, 2006) assessments. The IPCC (2013) assesses that climate sensitivity (defined in terms of a doubling of CO₂) is likely to be in the range 1.5 to 4.5 °C, very unlikely to be more than 6 °C, and extremely unlikely to be less than 1 °C.

Given the societal importance of climate sensitivity, it is unsurprising that many studies have turned to observations of past climates in an attempt to further refine, and test, estimates of this key parameter (e.g. see reviews by Rohling et al., 2018; Schmidt et al., 2014). Any such paleo-focussed attempt to characterise climate sensitivity requires knowledge of (a) the magnitude of the climatic response to a particular forcing and (b) the magnitude of the forcing itself. As such, many attempts to characterise climate sensitivity from the geological record have focussed on the relatively recent past, such as

49 the Last Glacial Maximum (LGM, e.g. Crucifix, 2006; Hansen et al., 2008; Hargreaves,
50 and M. Yoshimori, & Abe-Ouchi, 2012), or the Pleistocene (e.g. T. Friedrich, Timmer-
51 mann, Tigchelaar, Timm, & Ganopolski, 2016; Kohler et al., 2018) where datasets for
52 temperature change have relatively good spatial coverage, and the forcings are well un-
53 derstood and quantifiable. However, such studies still have relatively large uncertainties
54 due to difficulties associated with the interpretation of paleo proxy records, and/or have
55 often conflated feedbacks and forcings and so have either underestimated or overestimated
56 sensitivity (PALAEOSENS Project Members, 2012). Furthermore, the forcing during
57 the LGM and much of the Pleistocene was negative relative to modern, and so the rel-
58 evance for future climate change, where forcing is positive, may be limited. Other stud-
59 ies have focussed on warm periods within the last 5 million years, such as the Pliocene
60 (e.g. Hargreaves & Annan, 2016; Haywood et al., 2013; Lunt et al., 2010; Martínez-Botí
61 et al., 2015), when CO₂ concentrations were similar to that of today; however, even these
62 studies do not explore CO₂ concentrations of ~ 560 ppmv and above, that are more rel-
63 evant to climate sensitivity and typical end-of-century scenarios (Moss et al., 2010).

64 More recently, the community has started to move to ‘deep-time’ (here defined as
65 time periods older than ~ 5 million years ago) warm climates, during which CO₂ con-
66 centrations were very high (~ 1000 ppmv or more), in an attempt to find time periods
67 where the climate signal and forcings were largest, with the expectation that signal-to-
68 noise ratio will be reduced and climate sensitivity estimates will be more robust (e.g. Anag-
69 nostou et al., 2016; Cramwinckel et al., 2018; Shaffer, Huber, Rondanelli, & Pepke Ped-
70 ersen, 2016; Zeebe, Zachos, & Dickens, 2009). However, many such time periods were
71 essentially free from continental ice sheets, and tectonic changes over millions of years
72 mean that continental positions, mountain ranges and ocean bathymetry were all very
73 different compared to modern (e.g. Markwick, 2007). As such, it is possible that esti-
74 mates of paleo climate sensitivity from these time periods may have limited relevance
75 for assessing modern climate sensitivity, if climate sensitivity is paleogeography-dependent.
76 Furthermore, the upper end of CO₂ concentrations during many of these time periods
77 are so high that non-linearities in forcings and feedbacks (Bloch-Johnson, Pierrehum-
78 bert, & Abbot, 2015; Caballero & Huber, 2013) may further complicate their relation-
79 ship to the short-term future.

2 Methods

In order to explore the evolution of climate and climate sensitivity over geological timescales, we carry out an ensemble of 19 pairs of fully coupled atmosphere-ocean-vegetation climate model simulations with varying paleogeography and solar luminosity appropriate for each geological stage from the earliest Cretaceous (Berriasian stage, ~143 million years ago) to the latest Eocene (Priabonian stage, ~36 million years ago), at $\times 2$ and $\times 4$ preindustrial atmospheric CO_2 concentrations (i.e. 560 and 1120 ppmv).

The climate model, and the $\times 4$ simulations, are identical to those described in detail in Lunt et al. (2016), except that here they have been run for longer (10,422 years here compared with 1,422 years), in order to approach more closely to equilibrium. The $\times 2$ simulations are branched off from the $\times 4$ simulations after 422 years, and run for 10,000 years. The only difference between the simulation of each stage relative to another stage is the prescribed paleogeography (see Figure S1 in Supp Info of Lunt et al., 2016) and the solar constant (see Figure 2 of Lunt et al., 2016). All simulations have a modern astronomical configuration, and are initialised from a homogeneous global ocean salinity and an idealised zonal mean ocean temperature structure which is a cosine function of latitude (see Section 2.5 of Lunt et al., 2016).

The climate model used for the simulations is very similar to the HadCM3LM2.1E model described and evaluated in Valdes et al. (2017), except that we include a modification to the ozone profile to ensure that the model does not develop a runaway warming at $\times 4$ CO_2 , as discussed in Lunt et al. (2016). The model includes representations of ‘Charney’ feedbacks associated with changes in clouds, snow/seaice, lapse rate and water vapour, and the ‘Earth system’ feedback associated with changes in vegetation (Lunt et al., 2010), but does not include many other Earth system feedbacks associated with changes to, for example dust, methane, nitrogen dioxide, or ozone. The sign of many of these missing feedbacks is uncertain (IPCC, 2013), so it is not clear if our simulations will over or underestimate ‘true’ long-term Earth system sensitivity.

At the end of the model integration, all the simulations are very well spun up, with only small residual trends in ocean temperature, even in the deep ocean (the mean absolute global mean temperature trend at 2700 m depth of all simulations in the last 1000 years of simulation is 0.06°C per millennium; see Supp Info, Figure S1). In addition, Gregory plots (Gregory et al., 2004) of the energy balance at the top of the atmosphere (TOA)

112 against global mean surface temperature (Supp Info, Figure S2) show that the energy
 113 balance is very close to zero for all simulations, and that any residual energy balance is
 114 decreasing over time (the mean absolute TOA imbalance across all simulations is 0.036
 115 Wm^{-2} , and the maximum TOA imbalance is $+0.09 \text{ Wm}^{-2}$ in the Cenomanian at $\times 4$).
 116 However, there is a drift in the global mean salinity due primarily to the rigid-lid approx-
 117 imation in the ocean model, which includes minimum and maximum salinity thresholds
 118 (0 psu and 45 psu respectively). This, coupled with the presence of enclosed or restricted
 119 basins (such as the Arctic Ocean) with a net input of freshwater from the surrounding
 120 river catchments, means that the restricted basins become very fresh and reach the min-
 121 imum salinity threshold at the surface while the rest of the ocean tends to increase in
 122 salinity. We do not expect this drift to affect our results because (i) the absolute salin-
 123 ity does not have a strong effect on the density gradients due to the linearity of the equa-
 124 tion of state (Bryan & Cox, 1972) in the regime of the majority of the global ocean, (ii)
 125 the enclosed basins that reach the minimum salinity threshold have a relatively small
 126 area and do not affect the global ocean circulation, and (iii) the maximum salinity thresh-
 127 old is only reached in a few isolated gridcells in the tropics in the later Eocene simula-
 128 tions (Supp Info, Figure S3). Indeed, the mixed layer depths in our simulations (Supp
 129 info, Figure S6) are very similar to those presented in Lunt et al. (2016) (their Supp Info,
 130 Figure S10), indicating that the ocean circulation is relatively unchanged after 9,000 years,
 131 despite the gradual drift in salinity and gradually equilibrating temperatures.

132 **3 Results**

133 **3.1 Climate and climate sensitivity**

134 Figure 1a shows the global annual mean near-surface air temperature for the high
 135 ($\times 4$) and low ($\times 2$) CO_2 simulations (and see Table S1 in Supp Info). Both sets of sim-
 136 ulations show a similar trend (the r correlation coefficient between the two timeseries
 137 is 0.86; Supp info, Figure S4). In particular, there is a cooling in the very earliest Cre-
 138 taceous between the Berriasian and Valanginian at 140 Ma, a warming from ~ 130 to 90
 139 Ma peaking at the Turonian, and a cooling from 90 to 80 Ma to a minimum in the Cam-
 140 panian. In the Paleocene and Eocene the trends are less consistent across the two sets
 141 of simulations, but include a maximum in the Ypresian.

142 The global mean temperature in our $\times 4$ simulations has a greater total range across
143 the geological stages than that in the shorter simulations of Lunt et al. (2016) ($\sim 3^\circ\text{C}$
144 compared with $\sim 1^\circ\text{C}$; compare our Figure 1 with their Figures 5 and 7), and the regional
145 expression of this range also differs, but the main conclusion of Lunt et al. (2016), that
146 changes in paleogeography have a substantial effect on regional climate that must be con-
147 sidered when interpreting long proxy records, is robust.

148 Figure 1b shows the climate sensitivity of each stage (the difference in global mean
149 temperature between the $\times 2$ and $\times 4$ simulations); regional plots are shown in Supp Info,
150 Figure S5. The mean climate sensitivity over this period is 4.2°C , the minimum is 3.7°C
151 ($^\circ\text{C}$ (Berriasian stage, ~ 145 Ma) and the maximum is 5.3°C (Maastrichtian stage, ~ 70
152 Ma). The change in global climate sensitivity over time includes a gradual increase in
153 sensitivity from the earliest Cretaceous to the latest Cretaceous, a decrease to a mini-
154 mum in the Paleocene, and then an increase followed by a decrease in the Eocene. Our
155 modelled range of climate sensitivities in the Eocene (3.8 to 4.7°C) is consistent with es-
156 timates of 3.5 to 8.9°C (Cramwinckel et al., 2018) and 2.9 to 4.0°C (Anagnostou et al.,
157 2016), inferred from temperature and CO_2 proxies for this time period.

158 A quantitative analysis of the driving mechanisms is carried out in Section 3.2, but
159 in qualitative terms, the global mean temperature in the simulations appears to be driven
160 by a combination of CO_2 (explaining the offset in temperature between $\times 2$ and $\times 4$), in-
161 creasing solar constant (explaining a general increase in temperature from the earliest
162 Cretaceous to latest Eocene in both $\times 2$ and $\times 4$), plus a more variable signal that must
163 be associated with changing paleogeography. This paleogeographic signal appears to be
164 strongly related to the area of ocean in the prescribed paleogeographies (Figure 1c); the
165 ocean area correlates with both the $\times 4$ (r correlation coefficient = 0.63) and $\times 2$ simu-
166 lations (r correlation coefficient = 0.42). The mechanism for this paleogeographic forc-
167 ing is discussed in Section 3.2.

168 However, there are some differences between $\times 2$ and $\times 4$ that do not fit this qual-
169 itative relationship, and that can be seen in the evolution of climate sensitivity. In par-
170 ticular, there is a large swing in sensitivity around the Cretaceous-Paleocene boundary,
171 with relatively high sensitivity at the Maastrichtian and low sensitivity in the Selandian,
172 due to a relatively warm Maastrichtian at $\times 4$, and a relatively warm Selandian at $\times 2$
173 (Figure 1a,b). These anomalies are associated with changes in ocean circulation that take

174 place as a function of CO₂ at these two stages (Supp Info, Figure S6). The ocean cir-
 175 culation around this time has two possible states (i) a relatively warm global state char-
 176 acterised by deep water formation in the south Pacific Ocean, (Maastrichtian at ×4 and
 177 Selandian at ×2; Supp Info, Figure S6(b,g), and (ii) a relatively cold global state char-
 178 acterised by deep water formation in the south Atlantic and Indian Oceans (Maastrichtian
 179 at ×2 and Selandian at ×4; Supp Info, Figure S6(c,f)). Although changes in ocean cir-
 180 culation may not be expected to affect the global mean temperature to a great extent,
 181 in this case increased poleward heat transport in the Pacific basin results in a greater
 182 increase in global mean temperature than that caused by increased poleward heat trans-
 183 port in the Atlantic/ Indian basins. This enhanced Pacific poleward heat transport may
 184 be related to the greater areal extent of the Pacific basin, and is enhanced by sea ice albedo
 185 feedbacks around Antarctica. As such, the Cretaceous-Paleocene boundary is a partic-
 186 ularly sensitive time period to relatively small changes in paleogeography and/or CO₂,
 187 resulting in anomalously large or small climate sensitivities. For all other time periods,
 188 the deep water formation occurs in the same regions at ×4 as at ×2, although the re-
 189 gion varies as a function of paleogeography (e.g. in the South Atlantic in the Priabonian,
 190 Supp Info, Figure S6(a,e); in the North Pacific in the Berriasian, Supp Info, Figure S6(d,h)).

191 **3.2 Quantitative role of non-linear feedbacks in determining climate sen-** 192 **sitivity**

193 As well as the qualitative considerations above, a quantitative analysis of the sim-
 194 ulations is also possible. Here, we focus on the global mean response through applica-
 195 tion of a radiative forcing and feedback framework. Traditional linear radiative forcing
 196 theory (Hansen et al., 1984) states that if we choose one simulation as a reference state,
 197 all other simulations can be considered as a perturbation to this reference state, caused
 198 by a forcing F_{all} [Wm⁻²], where F_{all} is the sum of three separate forcings: F_{co2} due to
 199 a change in CO₂, F_{solar} due to a change in solar constant, and F_{geog} due to a change
 200 in paleogeography. Furthermore, the temperature difference relative to the reference state,
 201 ΔT , is given by

$$\Delta T = -\frac{F_{all}}{\lambda} = -\frac{F_{co2} + F_{solar} + F_{geog}}{\lambda}, \quad (1)$$

202 where λ , the feedback parameter [Wm⁻²K⁻¹], is negative. If we choose the Turonian at
 203 ×2 as our reference simulation, then F_{co2} is zero for all the ×2 simulations and equal to
 204 ΔR for all the ×4 simulations, where ΔR is the radiative forcing for a doubling of CO₂.

205 F_{solar} can be approximated by $(1 - \alpha_p)\Delta S_0/4$, where ΔS_0 is the change in solar con-
 206 stant relative to the Turonian and α_p is the planetary albedo. For the paleogeographic
 207 forcing, F_{geog} , the apparent importance of ocean area discussed in Section 3.1 suggests
 208 a role for surface albedo radiative forcing. Using a simple energy-balance model, Bar-
 209 ron, Sloan II, and Harrison (1980) showed that the albedo forcing, due to changes in con-
 210 tinental versus ocean area caused by changes in sea level, had a substantial effect on global
 211 mean temperature on geological timescales. The importance of ocean area through sur-
 212 face albedo forcing is also supported by more recent work (Pohl et al., 2019). However,
 213 others have suggested that the primary role of paleogeography on global mean temper-
 214 ature is through seasonality effects associated with the degree of fragmentation of con-
 215 tinents (Donnadieu, Pierrehumbert, Jacob, & Fluteau, 2006; Ladant & Donnadieu, 2016).
 216 Nonetheless, assuming changes in surface albedo to be the primary forcing due to pa-
 217 leogeography, F_{geog} can be approximated by $\Delta\alpha_s S_0/4$ where $\Delta\alpha_s$ is the change in sur-
 218 face albedo relative to the Turonian.

219 However, this linear framework predicts climate sensitivity to be constant over ge-
 220 ological time, because for each pair of $\times 2, \times 4$ simulations, the only difference in forcing
 221 is equal to ΔR , which is constant, giving a constant climate sensitivity of $-\Delta R/\lambda$. This
 222 is clearly at odds with the variable climate sensitivity in the full climate model (Figure
 223 1(c)), as also highlighted by the non-unity slope of the best-fit line between the $\times 2$ and
 224 $\times 4$ simulations (Supp Info Figure S4). As such, we introduce a non-linear parameter,
 225 a [$\text{Wm}^{-2}\text{K}^{-2}$], into Equation 1, following Bloch-Johnson et al. (2015), such that:

$$-F_{all} = \lambda\Delta T + a\Delta T^2. \quad (2)$$

226 The parameter a represents a temperature dependence (i.e. a non-linearity) of the strength
 227 of the feedbacks. Solving the resulting quadratic equation, and taking the physically re-
 228 alistic negative root, gives

$$\Delta T = \frac{-\lambda - \sqrt{\lambda^2 - 4a(F_{CO_2} + e_{solar}F_{solar} + e_{geog}F_{geog})}}{2a}, \quad (3)$$

229 where we have included factors e_{solar} and e_{geog} , which allow the efficacy (i.e. the tem-
 230 perature response due to a unit forcing, Hansen et al., 2005) of the solar and paleogeog-
 231 raphy terms to differ from that of CO_2 (for which the efficacy is equal to 1). In order
 232 to calculate the CO_2 forcing (F_{CO_2}) and the solar forcing (F_{solar}) we take $\Delta R = 3.7 \text{ Wm}^{-2}$
 233 (Houghton et al., 2001), and ΔS_0 from the solar constants prescribed in each simulation
 234 (Figure 1(d)). For the paleogeographic forcing (F_{geog}), we simply assume that the sur-

235 face albedo change, $\Delta\alpha_s = (\alpha_l - \alpha_o)\Delta A_o$ where $\alpha_l = 0.14$ and $\alpha_o = 0.06$ are typical
 236 global mean albedos of land and ocean respectively in the simulations, and ΔA_o is the
 237 relative change in area of ocean given in Figure 1(c). In order to account for the greater
 238 impact on radiative forcing of albedo changes in the tropics, we calculate the paleo-geo-
 239 graphic forcing as a function of latitude, accounting for varying incoming solar radiation,
 240 and weighting by area. This leaves Equation 3 with four unknowns; λ , a , e_{solar} , and e_{geog} .
 241 A minimal subjective tuning shows that $\lambda = -1 \text{ Wm}^{-2}\text{K}^{-1}$, $a = 0.04 \text{ Wm}^{-2}\text{K}^{-2}$, $e_{solar} =$
 242 0.7 , and $e_{geog} = 1.25$ gives a good qualitative match to our results for absolute tem-
 243 perature at $\times 2$ and $\times 4$, and climate sensitivity (Figure 1(a,b), light blue circles). Two
 244 exceptions are the Maastrichtian and Selandian stages, which we have already shown are
 245 associated with changes in the mode of ocean circulation, which are not captured in this
 246 simple forcings/feedbacks framework. We note that $\lambda = -1 \text{ Wm}^{-2}\text{K}^{-1}$ corresponds
 247 to a linear climate sensitivity of $3.7 \text{ }^\circ\text{C}$ per CO_2 doubling, which is within the range es-
 248 timated by the IPCC. We also note that $a = 0.04 \text{ Wm}^{-2}\text{K}^{-2}$ is within the range es-
 249 timated by Bloch-Johnson et al. (2015) of $-0.04 \leq a \leq 0.06 \text{ Wm}^{-2}\text{K}^{-2}$ from various
 250 climate model simulations carried out at multiple CO_2 concentrations. Finally, we note
 251 that a value of e_{geog} close to 1.0 also supports the assumption that surface albedo forc-
 252 ing associated with ocean area is a mechanism for variations in F_{geog} that is consistent
 253 with simple radiative forcing considerations. In principle, these four unknowns (λ , a , e_{solar} ,
 254 e_{geog}) could be objectively tuned to give a best fit to the data in Figure 1; however, here
 255 we are most interested in the general principle, which is that the evolution in climate sen-
 256 sitivity can be explained by non-linear feedbacks in the framework of Bloch-Johnson et
 257 al. (2015). It is worth noting that, as discussed by Bloch-Johnson et al. (2015), a neg-
 258 ative term inside the square root in Equation 3 can be interpreted as the system devel-
 259 oping a runaway greenhouse. For our values of λ and a , this occurs at a total forcing of
 260 $+6.25 \text{ Wm}^{-2}$ relative to the Turonian at $\times 2$, or about 1800 ppmv of CO_2 .

261 In order to explore the origin of these non-linear feedbacks on a global scale, we
 262 carry out a zonal-mean energy-balance analysis of the simulations, following Heinemann,
 263 Jungclaus, and Marotzke (2009). This shows that both albedo changes and emissivity
 264 changes contribute to the non-linearity in response to the solar and paleogeographic forc-
 265 ing. Given the relative warmth of the deep-time model simulations, it is likely that the
 266 non-linearity in albedo response is driven by non-linearities in short wave cloud feedbacks,

267 rather than snow and sea ice feedbacks. Indeed, regionally it is the tropics that domi-
268 nate the non-linearity in climate sensitivity (Supp Info, Figure S7a,b,c).

269 The changes in ocean area are dominated by changes in the Northern Hemisphere
270 mid-latitudes; the maximum in ocean area is during the Turonian (mid Cretaceous) when
271 the Western Interior Seaway in North America is extensive (see Figure S11 of Lunt et al.,
272 2016). The ocean area in the paleogeographies is consistent with sea level reconstruc-
273 tions of the Phanerozoic, such as Müller, Sdrolias, Gaina, Steinberger, and Heine (2008),
274 derived primarily from the age-area and depth-area distribution of the modern-day ocean
275 floor. These reconstructions also show a maximum in the mid Cretaceous; this agree-
276 ment is unsurprising given that sea-level reconstructions inform the production of the
277 paleogeographies. However, the details of the coastlines in the paleogeographies are un-
278 certain, in particular for greenhouse climates (Sømme, Helland-Hansen, & Granjeon, 2009).

279 Furthermore, the non-linearity found in our simulations supports previous stud-
280 ies that found that past climate sensitivity was a function of baseline CO₂ (e.g. Pohl,
281 Donnadieu, Le Hir, Buoncristiani, & Vennin, 2014, for the Ordovician), and suggests that
282 further non-linear behaviour would occur if we carried out simulations at $\times 1$ or $\times 8$ CO₂.

283 **3.3 Implications for assessment of future climate sensitivity**

284 It has been proposed that observational evidence of the climate sensitivity of the
285 past may be useful for constraining future climate sensitivity. To test this hypothesis,
286 we explore the relationship between modern and past climate sensitivity. To this end,
287 in addition to the Cretaceous, Paleocene, and Eocene simulations discussed above, we
288 also carry out a pair of Gelasian (early Pleistocene, ~ 2 Ma) simulations, spun up in an
289 identical manner to the other simulations, but at CO₂ concentrations of $\times 1$ and $\times 2$ (Fig-
290 ure 1(a)). The Gelasian is the closest available paleogeography to modern that has been
291 produced using the same procedures as the deep-time paleogeographies. In addition to
292 the solar constant, paleogeography and CO₂, this pair differs from the others in that it
293 has extensive Antarctic and Greenland ice sheets. The Gelasian climate sensitivity (3.7
294 °C) is at the lower end of the ensemble. Given the dependence of climate sensitivity on
295 temperature (i.e. the non-linearity of climate sensitivity) in the model simulations, this
296 implies that for the modern, the relatively small ocean area (Figure 1c) combined with
297 the presence of the Antarctic and Greenland ice sheets, more than offsets the relatively

298 high solar constant (Figure 1d), resulting in a relatively low climate sensitivity (and rel-
299 atively cold $\times 2$ simulation in the context of the increasing trend through the Cretaceous-
300 Paleocene-Eocene). The fact that CO_2 increases from $\times 1$ to $\times 2$ rather than $\times 2$ to $\times 4$
301 likely plays an additional role in the low modern sensitivity, through non-linearities in
302 both feedbacks and CO_2 forcing (Caballero & Huber, 2013). The regional expression of
303 climate sensitivity in the Gelasian includes an area of cooling in the north Pacific (Supp
304 Info, Figure S5a), but this does not appear to be associated with changes in deep wa-
305 ter formation. Cooling in this region is not seen in CO_2 -doubling model simulations as-
306 sociated with CMIP5 (IPCC, 2013). This could either be because the Gelasian has some
307 paleogeographic differences to modern (notably, land in the region of what is today the
308 Barents Sea, absence of a Hudson Bay, and a slightly open Panama Seaway), or because
309 these simulations are run much longer than CMIP5 simulations. If we take the Gelasian
310 results as representative of the modern climate sensitivity, then the implication is that
311 the use of observational geological data from the Cretaceous, Paleocene, or Eocene (e.g.
312 Anagnostou et al., 2016; Cramwinckel et al., 2018) to constrain future climate sensitiv-
313 ity should be carried out with care, and could in general lead to higher estimates than
314 are appropriate for modern. Indeed, the dependence of feedbacks on baseline temper-
315 ature highlighted in this work provide a plausible explanation for why Anagnostou et
316 al. (2016) found a higher climate sensitivity ($\sim 4^\circ\text{C}$ per CO_2 doubling) in the relatively
317 warm early Eocene climatic optimum than in the relatively cool late Eocene ($\sim 3^\circ\text{C}$ per
318 CO_2 doubling). Our findings are also consistent with Cramwinckel et al. (2018, their Ex-
319 tended Data Figure 9), who, relative to the late Eocene, find a higher sensitivity for the
320 warm EECO than for the cooler middle Eocene.

321 **3.4 Model evaluation: Inference of global mean temperature from single-** 322 **site proxy SST data, and comparison with benthic records**

323 The simulations cannot be directly evaluated with paleoclimate temperature data,
324 because CO_2 records of this time period are relatively uncertain (Foster, Royer, & Lunt,
325 2017). However, in combination with proxy sea surface temperature (SST) records de-
326 rived from planktic $\delta^{18}\text{O}$ from individual sites, the simulations can be used to infer a global
327 mean temperature, which can itself be compared with global mean temperature derived
328 from independent benthic $\delta^{18}\text{O}$ records (Figure 2), providing an evaluation of the regional
329 signals in the model simulations.

330 We assume that the global mean temperature and local SST scale linearly with each
 331 other, with a scaling factor derived from our model simulations at the two CO₂ concen-
 332 trations. As such, if the modelled temperature at the location of the proxy temperature
 333 (taking into account appropriate paleorotations due to plate movements), at the two dif-
 334 ferent CO₂ concentrations, is T^{2x} and T^{4x} , and the modelled global mean temperature
 335 at these CO₂ concentrations is $\langle T^{2x} \rangle$ and $\langle T^{4x} \rangle$, then the inferred global mean
 336 temperature, $\langle T \rangle^{inferred}$, can be derived from the proxy temperature estimate T_{proxy} ,
 337 as

$$\langle T \rangle^{inferred} = \langle T^{2x} \rangle + (T_{proxy} - T^{2x}) \frac{\langle T^{4x} \rangle - \langle T^{2x} \rangle}{T^{4x} - T^{2x}}. \quad (4)$$

338 Note that if the proxy temperature is greater than T^{4x} , or cooler than T^{2x} , then the in-
 339 ferred global mean is found by extrapolation rather than by interpolation, and is there-
 340 fore more uncertain (see Supp Info Figure S9). This is typically for inferred tempera-
 341 tures above about 23°C. The process is illustrated in Figure S9 in Supp Info for 3 sites.

342 We take T_{proxy} from planktic $\delta^{18}\text{O}$ estimates of Cretaceous, Paleocene and Eocene
 343 sea surface temperature (SST) compiled in O'Brien et al. (2017) (their Figure 9b) and
 344 Cramwinckel et al. (2018) (Supp Info, Figure S8(a); the modern site locations and their
 345 paleorotations are shown in Figure S8(b)). Prior to calculating $\langle T^{inferred} \rangle$, we re-
 346 move planktic $\delta^{18}\text{O}$ records from one location (Blake Nose, sites 1050 and 1052) that ap-
 347 pear exceptionally cold-biased, which we suggest potentially results from diagenesis. The
 348 $\langle T \rangle^{inferred}$ for each site is shown in Figure 2 as filled circles for each site (for some
 349 sites, the paleorotations do not extend back as far as the SST data; for these sites, shown
 350 as smaller circles, the last existing location is used), and the mean for each stage as an
 351 orange curve (including uncertainty estimates, see Figure S10 in Supp Info). The inferred
 352 global means from each site are less scattered than the SSTs from each site (Supp info
 353 Figure S8(a)), implying that our inference process has some skill in reconciling individ-
 354 ual SST records.

355 The inferred global mean temperature is for comparison with global mean temper-
 356 ature derived from the benthic $\delta^{18}\text{O}$ data of Cramer et al. (2011) and O. Friedrich et al.
 357 (2012), using the method of Hansen et al. (2013) in which benthic $\delta^{18}\text{O}$ is scaled to global
 358 mean temperature using a simple function that depends on the ice volume (Figure 2 in
 359 the main paper, grey lines). The $\langle T \rangle^{inferred}$ curve shows similar trends to the global
 360 mean surface temperature derived from benthic $\delta^{18}\text{O}$, namely, a maximum in the mid-

361 Cretaceous (Cenomanian, ~ 95 Ma), a secondary maximum in the early Eocene (Ypre-
362 sian, ~ 50 Ma), and a minimum in the latest Cretaceous (Maastrichtian, ~ 70 Ma). How-
363 ever, $\langle T \rangle^{inferred}$ is cooler than the central O. Friedrich et al. (2012) estimate by about
364 5°C . An offset is not surprising given that the Hansen et al. (2013) methodology makes
365 the simple assumption that changes in global mean surface temperature are identical to
366 changes in benthic ocean temperature prior to the Pliocene. In addition, the O. Friedrich
367 et al. (2012) benthic $\delta^{18}\text{O}$ data prior to the Paleocene could be regarded as represent-
368 ing an upper bound on temperature, because much of the warmest underlying data comes
369 from Demerara Rise which is bathed by a warm, saline water mass forming on the South
370 American shelf (O. Friedrich, Erbacher, Moriya, Wilson, & Kuhnert, 2008; MacLeod, Mar-
371 tin, & Blair, 2008). The cooling trend through the Eocene in our $\langle T \rangle^{inferred}$ is also
372 seen in the recent estimates of global mean temperature from Cramwinckel et al. (2018)
373 (blue line in Figure 2). However, our trend is less pronounced, being cooler in the early
374 Eocene (Ypresian) by about 6°C .

375 We also carry out the same process using a combined $\delta^{18}\text{O}$ and TEX_{86} dataset (Supp
376 Info, Figure S11), using TEX_{86} estimates compiled in O'Brien et al. (2017) (their Fig-
377 ure 9b), Inglis et al. (2015), and Cramwinckel et al. (2018), using a linear calibration (Supp
378 Info, Figure S11(a,b,c)) and an exponential calibration (Supp Info, Figure S11(c,d)). This
379 results in inferred temperatures with more variation across different sites than those from
380 solely $\delta^{18}\text{O}$, and in particular several sites give very warm inferred temperatures dur-
381 ing the Eocene, especially those from the southwest Pacific sector of the Southern Ocean
382 (e.g. ODP Site 1172, Hampden Beach, IODP Site 1356). This may result from a cold
383 model bias in the high latitudes, which has been noted in simulations of the early Eocene
384 with this model (Lunt et al., 2012), or a cold model bias in this particular region (Dou-
385 glas et al., 2014). However, it may also be in part due to possible seasonal biases in the
386 TEX_{86} data (Sluijs et al., 2006). This possibility is supported by the reversed meridional
387 temperature gradient implied in some sites in the raw TEX_{86} temperatures (e.g. site FL533
388 in the Campanian, or Mid Waipara in the Ypresian, Supp Info Figure S11(b)). This, com-
389 bined with recent discussions regarding the interpretation of the TEX_{86} proxy (Ho & Laep-
390 ple, 2016; Tierney, Damste, ad A. Sluijs, & Zachos, 2017), and the variety of published
391 calibrations (see overview in Inglis et al. (2015)), makes interpretation of the resulting
392 apparent inconsistencies challenging. However, it is worth noting that our estimates of
393 inferred global mean temperature from the TEX_{86} proxy at ODP Site 959 in the Eocene

394 are in remarkable agreement with those inferred by Cramwinckel et al. (2018) (Supp Info
395 Figure S11(a)).

396 4 Conclusions

397 In summary, modelled climate sensitivity varies through the Cretaceous-Paleocene-
398 Eocene from about 3.5 to about 5.5 °C. This variation is explained by a combination of
399 the changing background forcing through this time period due to gradually increasing
400 solar luminosity and varying ocean area, and non-linearities in water vapour and short-
401 wave cloud feedbacks. The maximum in sensitivity in the Maastrichtian can be explained
402 through a combination of its high ocean area and reasonably high solar luminosity, com-
403 bined with a switch in the mode of ocean circulation. The modern climate sensitivity
404 is relatively low in this context, despite the high solar luminosity, due to its low atmo-
405 spheric CO₂ baseline, relatively small ocean area, and the presence of ice sheets. The
406 model simulations that underpin these findings cannot be directly evaluated, but the re-
407 lationship between simulated local and global mean temperatures is consistent with proxy
408 δ¹⁸O estimates of SST and deep ocean temperatures. Finally, in the context of future
409 climate sensitivity, this work supports the importance of studies exploring non-linearities
410 in feedbacks and climate sensitivity in the framework of nonlinMIP (Good et al., 2016).

411 Acknowledgments

412 We acknowledge support from the UK National Environmental Council grants NE/K014757/1,
413 NE/I005722/1, NE/I005714/1, NE/K012479/1, NE/I005501/2, and NE/P01903X/1. R.D.P
414 acknowledges ERC Grant 340923 (TGRES). Figures S1 to S11 are available in Support-
415 ing Information. The output from the model simulations is available from [https://www](https://www.paleo.bristol.ac.uk/ummodel/scripts/papers/[tobecompleted])
416 [.paleo.bristol.ac.uk/ummodel/scripts/papers/\[tobecompleted\]](https://www.paleo.bristol.ac.uk/ummodel/scripts/papers/[tobecompleted]).

417 References

- 418 Anagnostou, E., John, E., Edgar, K., Foster, G., Ridgwell, A., Inglis, G., ... Pear-
419 son, P. (2016). Changing atmospheric co2 concentration was the primary
420 driver of early cenozoic climate. *Nature*. doi: 10.1038/nature17423
- 421 Barron, E. J., Sloan II, J. L., & Harrison, C. G. A. (1980). Potential significance of
422 land-sea distribution and surface albedo variations as a climatic forcing factor;
423 180 m.y. to the present. *Palaeogeography, Palaeoclimatology, Palaeoecology*, 30,

424 17-40.

425 Bloch-Johnson, J., Pierrehumbert, R. T., & Abbot, D. S. (2015). Feedback tem-
426 perature dependence determines the risk of high warming. *Geophysical Research*
427 *Letters*, *42*, 4973-4980. Retrieved from doi:10.1002/2015GL064240

428 Bryan, K., & Cox, M. D. (1972). An approximate equation of state for numerical
429 models of ocean circulation. *J. Phys. Oceanogr.*, *2*, 510-514.

430 Caballero, R., & Huber, M. (2013). State-dependent climate sensitivity in past
431 warm climates and its implications for future climate projections. *Proc Natl*
432 *Acad Sci*, *110*, 14162-14167.

433 Charney, J., Arakawa, A., Baker, D. J., Bolin, B., Dickinson, R. D., Goody, R. M.,
434 ... Wunsch, C. I. (1979). *Carbon dioxide and climate: A scientific assessment*.
435 National Research Council.

436 Cramer, B. S., Miller, K. G., Barrett, P. J., & Wright, J. D. (2011). Late cretaceous-
437 neogene trends in deep ocean temperature and continental ice volume: Rec-
438 onciling records of benthic foraminiferal geochemistry ($\delta^{18}\text{O}$ and mg/ca)
439 with sea level history. *Journal of Geophysical Research*, *116*, C12023. doi:
440 10.1029/2011JC007255

441 Cramwinckel, M. J., Huber, M., I. J. K., Agnini, C., Bijl, P. K., Bohaty, S. M., ...
442 Sluijs, A. (2018). Synchronous tropical and polar temperature evolution in the
443 eocene. *Nature*, *559*, 382-386.

444 Crucifix, M. (2006). Does the last glacial maximum constrain climate sensitivity?
445 *Geophysical Research Letters*, *33*. doi: 10.1029/2006GL027137

446 Donnadieu, Y., Pierrehumbert, R., Jacob, R., & Fluteau, F. (2006). Modelling the
447 primary control of paleogeography on cretaceous climate. *Earth and Planetary*
448 *Science Letters*, *248*, 426-437.

449 Donner, S. D., Skirving, W. J., Little, C. M., Oppenheimer, M., & Hoegh-Guldberg,
450 O. (2005). Global assessment of coral bleaching and required rates of adapta-
451 tion under climate change. *Global Change Biology*, *11*, 2251-2265.

452 Douglas, P. M. J., Affek, H. P., Ivany, L. C., Houben, A. J. P., and A. Sluijs,
453 W. P. S., Schouten, S., & Pagani, M. (2014). Pronounced zonal hetero-
454 geneity in eocene southern high-latitude sea surface temperatures. *PNAS*, *111*,
455 6582-6587.

456 Foster, G. L., Royer, D. L., & Lunt, D. J. (2017). Future climate forcing poten-

- 457 tially without precedent in the last 420 million years. *Nature Communications*,
 458 8. doi: 10.1038/ncomms14845
- 459 Friedrich, O., Erbacher, J., Moriya, K., Wilson, P., & Kuhnert, H. (2008). Warm
 460 saline intermediate waters in the cretaceous tropical atlantic ocean. *Nature*
 461 *Geoscience*, 1, 453-457.
- 462 Friedrich, O., Norris, R., & Erbacher, J. (2012). Evolution of middle to late creta-
 463 ceous oceans - a 55 m.y. record of earth's temperature and carbon cycle. *Geol-*
 464 *ogy*, 40, 107-110.
- 465 Friedrich, T., Timmermann, A., Tigchelaar, M., Timm, O. E., & Ganopolski, A.
 466 (2016). Nonlinear climate sensitivity and its implications for future greenhouse
 467 warming. *Science Advances*, 2. doi: 10.1126/sciadv.1501923
- 468 Good, P., Andrews, T., Chadwick, R., Dufresne, J.-L., Gregory, J. M., Lowe, J. A.,
 469 ... Shiogama, H. (2016). nonlinmip contribution to cmip6: model intercom-
 470 parison project for non-linear mechanisms: physical basis, experimental design
 471 and analysis principles (v1.0). *Geoscientific Model Development*, 9(11), 4019-
 472 4028. Retrieved from <https://www.geosci-model-dev.net/9/4019/2016/>
 473 doi: 10.5194/gmd-9-4019-2016
- 474 Gregory, J. M., W. J. Ingram, W. J., Palmer, M. A., Jones, G. S., Stott, P. A.,
 475 Thorpe, R. B., ... Williams, K. D. (2004). A new method for diagnosing
 476 radiative forcing and climate sensitivit. *Geophysical Research Letters*, 31,
 477 L03205. doi: 10.1029/2003gl018747
- 478 Hansen, J., Lacis, A., Rind, D., Russell, G., Stone, P., Fung, I., ... Lerner, J.
 479 (1984). Climate sensitivity: Analysis of feedback mechanisms. In J. E. Hansen
 480 & T. Takahashi (Eds.), *Climate processes and climate sensitivity* (p. 130-163).
 481 American Geophysical Union.
- 482 Hansen, J., Sato, M., Kharecha, P., Beerling, D., Berner, R., Masson-Delmotte, V.,
 483 ... Zacher, J. C. (2008). Target atmospheric CO₂: Where should humanity
 484 aim? *The Open Atmospheric Science Journal*, 2, 217-231.
- 485 Hansen, J., Sato, M., Ruedy, R., Nazarenko, L., Lacis, A., Schmidt, G. A., ...
 486 Zhang, S. (2005). Efficacy of climate forcings. *Journal of Geophysical Re-*
 487 *search*, 110, doi:10.1029/2005JD005776.
- 488 Hansen, J., Sato, M., Russell, G., & Kharecha, P. (2013). Climate sensitivity, sea
 489 level and atmospheric carbon dioxide. *Phil. Trans. R. Soc. A*, 371.

- 490 Hargreaves, J. C., and M. Yoshimori, J. D. A., & Abe-Ouchi, A. (2012). Can the
491 last glacial maximum constrain climate sensitivity? *Geophysical Research Let-*
492 *ters*, *39*. doi: doi:10.1029/2012GL053872
- 493 Hargreaves, J. C., & Annan, J. D. (2016). Could the pliocene constrain the equilib-
494 rium climate sensitivity? *Climate of the Past*, *12*(8), 1591–1599. doi: 10.5194/
495 cp-12-1591-2016
- 496 Haywood, A. M., Hill, D. J., Dolan, A. M., Otto-Bliesner, B. L., Bragg, F., Chan,
497 W.-L., ... Zhang, Z. (2013). Large-scale features of pliocene climate: results
498 from the pliocene model intercomparison project. *Climate of the Past*, *9*(1),
499 191–209. Retrieved from <https://www.clim-past.net/9/191/2013/> doi:
500 10.5194/cp-9-191-2013
- 501 Heinemann, M., Jungclaus, J. H., & Marotzke, J. (2009). Warm Paleocene/Eocene
502 climate as simulated in ECHAM5/MPI-OM. *Climate of the Past*, *5*, 785-802.
- 503 Ho, S. L., & Laepple, T. (2016). Flat meridional temperature gradient in the early
504 eocene in the subsurface rather than surface ocean. *Nature Geoscience*, *9*, 606-
505 610.
- 506 Hope, C. (2006). The marginal impact of co2 from page2002: An integrated as-
507 sessment model incorporating the ipccs five reasons for concern. *The Integrated*
508 *Assessment Journal*, *6*, 19-56.
- 509 Houghton, J. T., Ding, Y., Griggs, D. J., Noguer, M., van der Linden, P. J., Dai,
510 X., ... Johnson, C. A. (2001). *Climate change 2001: The scientific basis*.
511 Cambridge University Press.
- 512 Inglis, G. N., Farnsworth, A., Lunt, D., Foster, G., Hollis, C., Pagani, M., ...
513 Pancost, R. (2015). Descent towards the icehouse: Eocene sea sur-
514 face cooling inferred from gdgt distributions. *Paleoceanography*, *30*,
515 doi:10.1002/2014PA002723.
- 516 IPCC. (2013). *Climate change 2013: The physical science basis*. Cambridge Univer-
517 sity Press.
- 518 Kohler, P., Knorr, G., Stap, L. B., Ganopolski, A., de Boer, B., van de Wal,
519 R. S. W., ... Rupke, L. H. (2018). The effect of obliquitydriven changes
520 on paleoclimate sensitivity during the late pleistocene. *Geophysical Research*
521 *Letters*, *45*, 6661-6671.
- 522 Ladant, J.-B., & Donnadiou, Y. (2016). Palaeogeographic regulation of glacial events

- 523 during the cretaceous supergreenhouse. *Nature Communications*, *7*, 1-9. doi:
 524 10.1038/ncomms12771
- 525 Lunt, D. J., Dunkley Jones, T., Heinemann, M., Huber, M., LeGrande, A., Winguth,
 526 A., ... Winguth, C. (2012). A model-data comparison for a multi-model en-
 527 semble of early eocene atmosphere-ocean simulations: EoMIP. *Climate of the*
 528 *Past*, *8*(5), 1717–1736.
- 529 Lunt, D. J., Farnsworth, A., Loftson, C., Foster, G. L., Markwick, P., O'Brien,
 530 C. L., ... Wrobel, N. (2016). Palaeogeographic controls on climate and proxy
 531 interpretation. *Climate of the Past*, *12*(5), 1181–1198.
- 532 Lunt, D. J., Haywood, A. M., Schmidt, G. A., Salzmann, U., Valdes, P. J., &
 533 Dowsett, H. J. (2010). Earth system sensitivity inferred from Pliocene mod-
 534 elling and data. *Nature Geoscience*, *3*, 60-64.
- 535 MacLeod, K., Martin, E. E., & Blair, S. W. (2008). Nd isotopic excursion across
 536 cretaceous ocean anoxic event 2 (cenomanian-turonian) in the tropical north
 537 atlantic. *Geology*, *36*, 811-814.
- 538 Markwick, P. J. (2007). Deep time perspectives on climate change: marrying the
 539 signal from computer models and biological proxies. In M. W. M, A. M. Hay-
 540 wood, J. F. Gregory, & D. N. Schmidt (Eds.), (chap. The palaeogeographic
 541 and palaeoclimatic significance of climate proxies for data-model comparisons).
 542 The Micropalaeontological Society Special Publications, Geological Society of
 543 London.
- 544 Martínez-Botí, M., Foster, G., Chalk, T., Rohling, E., Sexton, P., Lunt, D., ...
 545 Schmidt., D. (2015). Plio-pleistocene climate sensitivity evaluated using
 546 high-resolution co2 records. *Nature*, *518*.
- 547 Moss, R. H., Edmonds, J. A., Hibbard, K. A., Manning, M. R., Rose, S. K., van
 548 Vuuren, D. P., ... Wilbanks, T. J. (2010). The next generation of scenarios for
 549 climate change research and assessment. *Nature*, *463*, 747-756.
- 550 Müller, R. D., Sdrolias, M., Gaina, C., Steinberger, B., & Heine, C. (2008). Long-
 551 term sea-level fluctuations driven by ocean basin dynamics. *Science*, *319*,
 552 1357-1362. doi: 10.1126/science.1151540
- 553 O'Brien, C. L., Robinson, S. A., Pancost, R. D., Damst, J. S. S., Schouten, S., Lunt,
 554 D. J., ... Wrobel, N. E. (2017). Cretaceous sea-surface temperature evolution:
 555 Constraints from tex86 and planktonic foraminiferal oxygen isotopes. *Earth*

- 556 *Science Reviews*, 172, 224-247.
- 557 PALAEOSENS Project Members. (2012). Making sense of palaeoclimate sensitivity.
558 *Nature*, 491, 683-691.
- 559 Pohl, A., Donnadieu, Y., Le Hir, G., Buoncristiani, J.-F., & Vennin, E. (2014). Ef-
560 fect of the ordovician paleogeography on the (in)stability of the climate. *Cli-*
561 *mate of the Past*, 10(6), 2053–2066. Retrieved from [https://www.clim-past](https://www.clim-past.net/10/2053/2014/)
562 [.net/10/2053/2014/](https://www.clim-past.net/10/2053/2014/) doi: 10.5194/cp-10-2053-2014
- 563 Pohl, A., Laugie, M., Borgomano, J., Michel, J., Lanteaume, C., Scotese, C. R.,
564 ... Donnadieu, Y. (2019). Quantifying the paleogeographic driver of cre-
565 taceous carbonate platform development using paleoecological niche model-
566 ing. *Palaeogeography, Palaeoclimatology, Palaeoecology*, 514, 222 - 232. doi:
567 <https://doi.org/10.1016/j.palaeo.2018.10.017>
- 568 Rogelj, J., Meinshausen, M., Sedlacek, J., & Knutti, R. (2014). Implications of po-
569 tentially lower climate sensitivity on climate projections and policy. *Environ-*
570 *mental Research Letters*, 9. doi: doi:10.1088/1748-9326/9/3/031003
- 571 Rohling, E. J., Marino, G., Foster, G. L., Goodwin, P. A., von der Heydt, A. S., &
572 Kohler, P. (2018). Comparing climate sensitivity, past and present. *Annual*
573 *Review of Marine Science*, 10, 261-288.
- 574 Schmidt, G. A., Annan, J. D., Bartlein, P. J., Cook, B. I., Guilyardi, E., Hargreaves,
575 J. C., ... Yiou, P. (2014). Using palaeo-climate comparisons to constrain fu-
576 ture projections in cmip5. *Climate of the Past*, 10(1), 221–250. Retrieved from
577 <https://www.clim-past.net/10/221/2014/> doi: 10.5194/cp-10-221-2014
- 578 Shaffer, G., Huber, M., Rondanelli, R., & Pepke Pedersen, J. O. (2016). Deep time
579 evidence for climate sensitivity increase with warming. *Geophysical Research*
580 *Letters*, 43(12), 6538-6545. doi: 10.1002/2016GL069243
- 581 Sluijs, A., Schouten, S., Pagani, M., Woltering, M., Brinkhuis, H., Damst, J. S., &
582 ... Moran, K. (2006). Subtropical Arctic Ocean temperatures during the
583 Palaeocene/Eocene thermal maximum. *Nature*, 441, 610-613.
- 584 Sømme, T., Helland-Hansen, W., & Granjeon, D. (2009). Impact of eustatic ampli-
585 tude variations on shelf morphology, sediment dispersal, and sequence strati-
586 graphic interpretation: Icehouse versus greenhouse systems. *Geology*, 37(7),
587 587-590. doi: 10.1130/G25511A.1
- 588 Tierney, J. E., Damste, J. S. S., ad A. Sluijs, R. D. P., & Zachos, J. C. (2017).

- 589 Eocene temperature gradients. *Nature Geoscience*, *10*, 538-539.
- 590 Valdes, P. J., Armstrong, E., Badger, M. P. S., Bradshaw, C. D., Bragg, F., Cruci-
591 fix, M., ... Williams, J. H. T. (2017). The bridge hadcm3 family of climate
592 models: Hadcm3@bristol v1.0. *Geoscientific Model Development*, *10*(10),
593 3715–3743. doi: 10.5194/gmd-10-3715-2017
- 594 Zeebe, R. E., Zachos, J. C., & Dickens, G. R. (2009). Carbon dioxide forcing alone
595 insufficient to explain palaeoceneocene thermal maximum warming. *Nature*
596 *Geoscience*, *2*, 576-580.

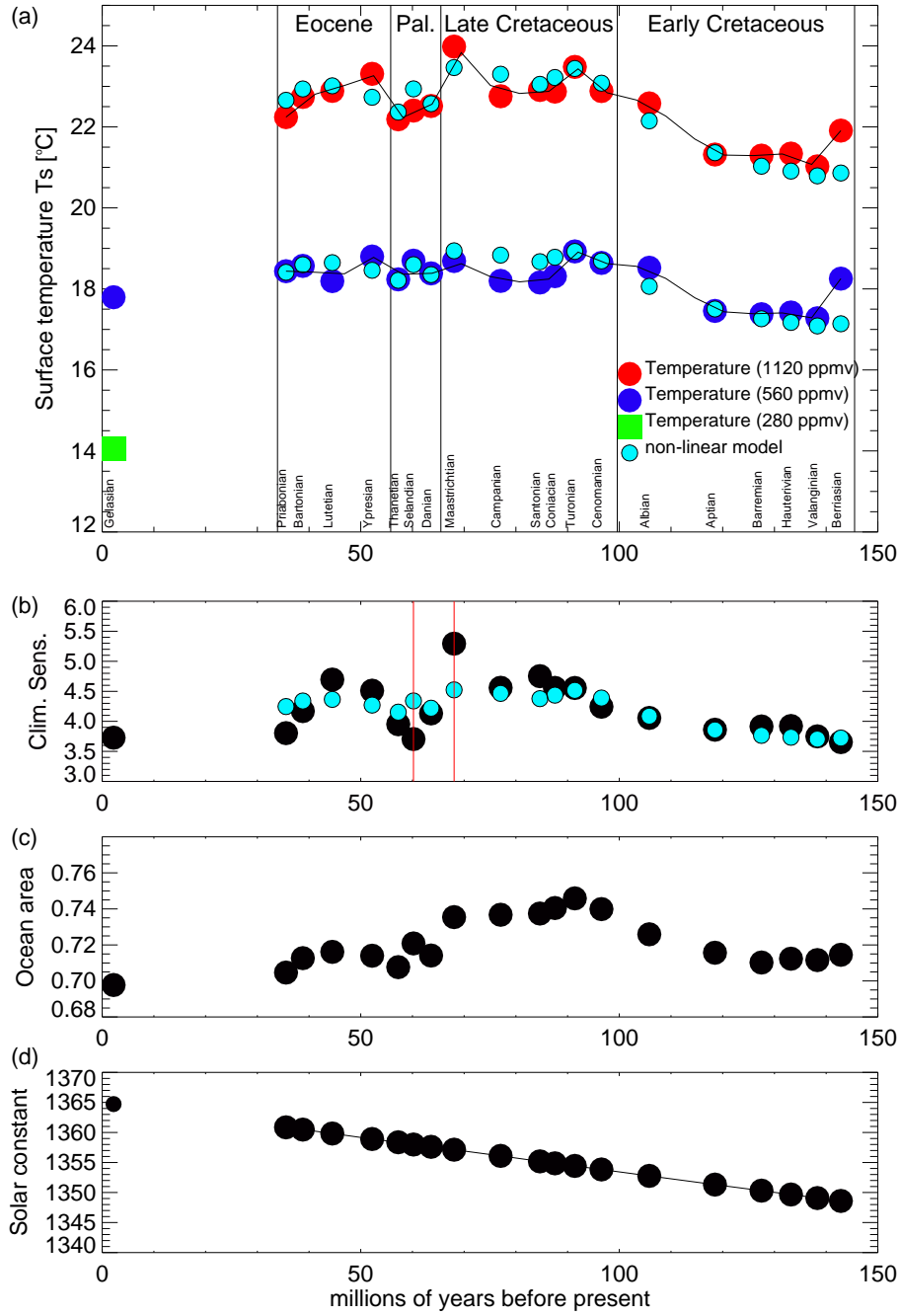


Figure 1. (a) Global annual mean near-surface air temperature in the $\times 2$ (dark blue circles) and $\times 4$ (red circles) CO₂ simulations, and the Gelasian $\times 1$ simulation (green square). For each set of simulations the curved black line is a spline fit to the data, of resolution about 5 million years. The non-linear model fit to the $\times 2$, $\times 4$ simulations is shown with light blue circles. (b) Global mean climate sensitivity (i.e. $\times 4$ minus $\times 2$) over time (black circles). Non-linear model sensitivity is shown with light blue circles. Red vertical lines show those time periods that have a switch in ocean circulation between the $\times 2$ and $\times 4$ simulations. (c) Ocean area over time (as a fraction of the global surface area, calculated from the paleogeographies at the model resolution). (d) Solar constant over time [Wm^{-2}].

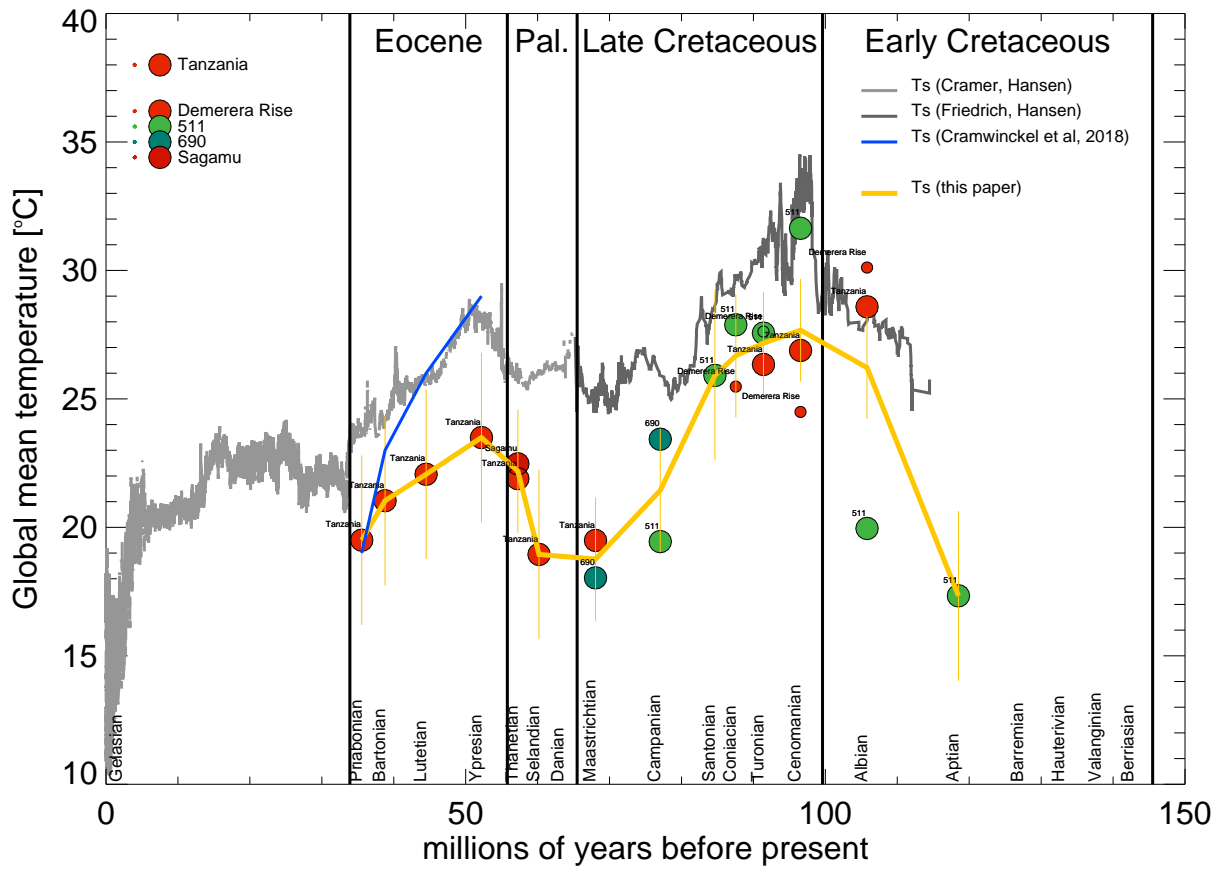


Figure 2. Filled circles show the global mean temperature inferred from the model simulations and planktic $\delta^{18}\text{O}$ SST estimates from the sites in Supp Info Figure S8 (using Equation 4, as illustrated in Figure S9 in Supp Info). The colour corresponds to the modern latitude of each site, with warm colours for low latitudes and cold colours for high latitudes. Smaller circles are those sites where the paleorotations are approximate. The orange curve shows the mean inferred temperature for each geological stage, with uncertainty bars according to the number of sites (see Supp info Figure S10). The grey lines are global mean temperatures estimated from the Cramer et al. (2011) (light grey) and O. Friedrich et al. (2012) (dark grey) benthic $\delta^{18}\text{O}$ datasets, using the method of Hansen et al. (2013). The blue line shows global mean temperatures in the Eocene from Cramwinckel et al. (2018).